The influence of fibre alignment on the fracture toughness of anisotropic soft tissue

Ankit Baranwal[a], Prabhat K. Agnihotri[a,*], J. P. McGarry[b]

[a]Mechanics of Advanced Materials Laboratory, Department of Mechanical Engineering, Indian Institute of Technology, Ropar, Punjab, India.

[b]Biomedical Engineering, National University of Ireland, Galway, Galway, Ireland.

*Corresponding author: prabhat@iitrpr.ac.in

Abstract

Finite element (FE) simulations are performed to investigate the effect of fiber induced anisotropy on the notch behavior in hyperelastic skin type materials. The modified anisotropic (MA) model is used to define the constitutive behavior in FE simulations through Abaqus user defined material model UMAT. A parametric study is carried out to examine the effect of fiber orientation, notch root radius and sample geometry on the stress field ahead of the notch tip. A non-dimensional parameter ξ is defined to characterize the combined effect of J energy and average anisotropic energy $(\phi_{aniso})_{avg}$ on the notch behavior. It is shown that fibre orientation significantly influences the stress state and J-integral at the notch. The findings of the present study will be helpful in determining optimal constitution and orientation of skin grafts at locations of high stress and complex geometries, such as corner of eyes and lips etc.

Keywords: Skin type materials; notch; J – integral; arterial tissue; tearing strength.

1. Introduction

Understanding the deformation and fracture behavior of soft tissues and skin type materials is important to avoid their damage and to develop efficient healing strategies. Moreover, designing artificial skin with sensing capabilities is one of the critical requirements to fabricate soft grippers and muscles used in medical robots. Use of hyperelastic materials like polydimethylsiloxane (PDMS) as artificial muscles and skin is widely reported in literature [1-3]. Human as well as artificial skin are often subjected to lacerations and wounds by the blunt objects such as paper, corner of sheet metal component, nails and fasteners, blade cuts etc. causing skin damage and failure [4]. Therefore, it is essential to understand the behavior of notches to improve the failure resistance of skin type materials [5]. The skin type materials essentially consists of anisotropic fiber embedded in an isotropic hyperelastic matrix. Thus, the fiber induced anisotropy significantly affects the average response of soft tissues to the applied loading. The constitutive relation developed by Holzapfel et al. [6] (HGO model) is most widely used model to study the deformation behavior of anisotropic soft tissues [7-10]. In this model, a strain energy density function for hyperelastic (soft elastin) materials reinforced by two families of stiffer (collagen) fibers is introduced. The total strain energy has two contributions, namely: (1) an anisotropic contribution from the reinforcing fibers, and (2) an isotropic contribution from the ground matrix. Nolan *et al*. [11] proposed a modification of the HGO model so that it accurately and robustly models compressible or near incompressible anisotropic soft tissue. In short, this requires the use of the full anisotropic invariants, rather than isochoric anisotropic invariants. The authors demonstrate that incorrect use of isochoric anisotropic invariants can generate dramatic errors, even for cases of near-incompressible materials. Even though anisotropic hyperelastic models have been used for a wide range of diverse biomechanical applications [12-19], no previous study, to the best of the authors' knowledge, has investigated the behavior of notches in anisotropic hyperelastic skin type materials. The need for such an analysis is further motivated by the experimental study by Yang *et al*. [20] of edge cracks in skin composed of collagen fiber and elastin. It is reported that tensile loading results in crack blunting in rabbit skin. It is suggested that fibril straightening, fibril reorientation along the loading direction, elastic stretching and interfibrillar sliding contribute to the redistribution of stresses ahead of the notch tip and leads to extremely high tearing strength of skin as schematically presented in Fig. 1 [20]. Apart from numerical and experimental studies, theoretical models are also developed to account for the fiber induced toughening in soft tissues [21, 22] such as crack bridging model proposed by Meng *et al*. [23]. However, there are still unresolved questions such as: does fiber orientation in front of the notch tip really increase fracture resistance? How does fiber induced anisotropy contribute to the stress ahead of the notch tip in soft tissues (see Fig. 1)? An attempt has been made in this study to address these questions.

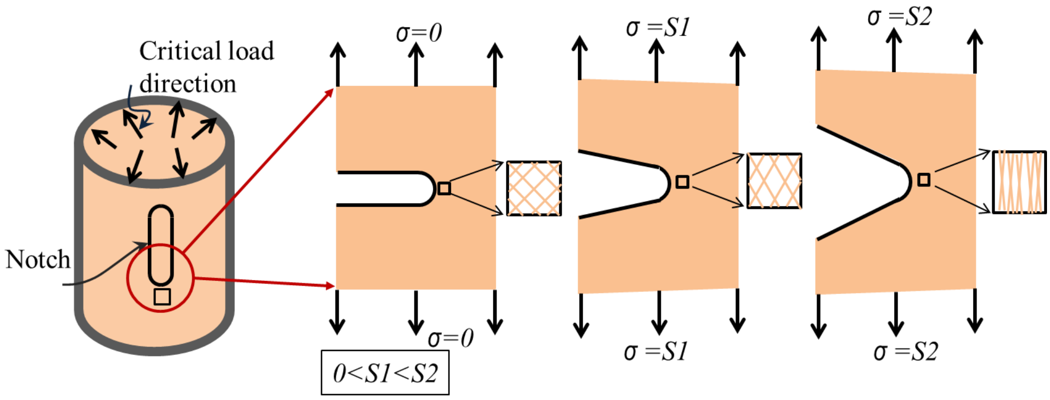

Fig. 1: Schematic showing arterial wall with notch along longitudinal direction and blunting of notch caused due to reorientation of fibers ahead of the notch tip under opening mode loading.

The primary objective of the present study is to advance the current understanding of the role of fiber alignment as a toughening mechanism in anisotropic hyperelastic materials. To this end, the effect of fiber orientation on the notch tip stress is investigated using the MA model [11]. The *J*-integral is used to compare the relative fracture resistance for a range of cases [24, 25]. It is shown that notch tip stress and resistance to crack propagation of anisotropic hyperelastic materials critically depends on the fiber alignment. The insights gained from this analysis are applicable to design artificial skin with improved tearing strength and fracture toughness.

2. Material model

The MA model developed by Nolan *et al*. [11], which is a modified form of the HGO model to correctly simulate compressible or near-incompressible anisotropic hyperelastic material behavior, is used in the current study to examine the notch behavior in anisotropic hyperelastic materials [26]. Briefly, two families of anisotropic fibers with orientations given by vectors $\widehat{a_{04}}$ and $\widehat{a_{06}}$ are embedded in a hyperelastic isotropic matrix. The total strain energy is composed of volumetric and isochoric contributions from the isotropic matrix, in addition to the anisotropic strain energy due to fibers as described in equation (1).

$$\phi(\mathcal{J}, \boldsymbol{C}, \widehat{a_{04}}, \widehat{a_{06}}) = \phi_{vol}(\mathcal{J}) + \phi_{iso}(\mathcal{J}, \boldsymbol{C}) + \phi_{aniso}(\boldsymbol{C}, \widehat{a_{04}}, \widehat{a_{06}}), \quad (1)$$

The isotropic part $\phi_{vol}(\mathcal{J}) + \phi_{iso}(\mathcal{J}, \boldsymbol{C})$ is given by a neo-Hookean model for slightly compressible hyper-elastic material and defined using a bulk modulus (k_0) and a shear modulus (μ_0).

$$\phi_{vol}(\mathcal{J}) = \frac{1}{2} k_0 (\mathcal{J} - 1)^2 \;\; ; \quad \phi_{iso}(\mathcal{J}, \boldsymbol{C}) = \frac{1}{2} \mu_0 (\bar{I}_1 - 3). \quad (2)$$

$\mathcal{J}$ is the determinant of deformation gradient tensor $\boldsymbol{F}$ and $\boldsymbol{C}$ is Right Cauchy-Green tensor, and $\bar{I}_1$ is the isochoric part of I_1 and defined as $\bar{I}_1 = \mathcal{J}^{-2/3} I_1$. The form of ϕ_{aniso} is given as,

$$\phi_{\text{aniso}}(\boldsymbol{C}, \widehat{a_{04}}, \widehat{a_{06}}) = \frac{k_1}{2k_2} \sum_{i=4,6} \{\exp[k_2 (I_i - 1)^2] - 1\}, \quad (3)$$

noting that the anisotropic contribution is not decomposed into separate isochoric and volumetric contributions in the MA model, but rather uses the full form of the I_4 and I_6 invariants. $\widehat{a_{04}}, \widehat{a_{06}}$ denote the unit vectors along fiber direction. I_1, I_4, I_6 are the invariants with $I_1 = tr(\boldsymbol{C})$, $I_4 = \widehat{a_{04}}.(\boldsymbol{C}\widehat{a_{04}})$, $I_{06} = \widehat{a_{06}}.(\boldsymbol{C}\widehat{a_{06}})$. Two positive material constants k_1 and k_2 define property of fiber family. The exponential form of fibre strain stiffening originally proposed in the HGO model is motivated by the uncoiling of collagen fibres during extension. Furthermore, fibres are not assumed to contribute mechanically if shortening (I_4, $I_6 < 1$) to represent fibre buckling under compression. The Cauchy stress is calculated from energy density ϕ,

$$\boldsymbol{\sigma} = \frac{1}{J}\boldsymbol{F}\frac{\partial\phi}{\partial\boldsymbol{F}}\,. \tag{4}$$

A modified version of user defined material model UMAT developed in [11] is used here in finite element (FE) simulations performed with commercially available FE software Abaqus [27].

3. Computational model

The effect of notch geometry and fiber orientation on the notch tip stress and fracture energy is parametrically investigated through a series of FE simulations. The geometry of single edge U-notch specimen is shown in Fig. 2. The notch is aligned in the direction – 1. Geometric dimensions of the numerical model are in term of notch root radius *r*, initial notch length *a*, specimen width *w* and height *h* are given in Table 1. The thickness of the model is kept constant at 1 mm in all the simulations.

Table 1: Geometry of the computational model used in FE analysis.

a	*h*	*w*	*r*	*r/a*	*a/w*	*h/w*
10	200	100	0.1, 1, 10	0.01, 0.1, 1	0.1	2

Due to the symmetry, only half domain is modeled (see Fig. 2(b)). The bottom edge is fixed in the direction – 2; a displacement u_2 = 0.1 mm is applied at the top edge in the direction perpendicular to the notch length. To ensure plane strain deformation, the displacement u_3=0 is imposed on the front and back surfaces. The model is meshed using C3D8 element with single element in the thickness direction. While a finer mesh is used closer to notch tip, a coarser element size is specified away from the notch root to reduce the computational time (see Fig. 3). Moreover, the mesh is varied close to notch root such that the ratio of element size to notch root radius is less than 0.1 in all the cases. The constitutive behaviour of skin type material is integrated into the FE standard implicit solver of Abaqus through a user defined material subroutine (UMAT). The material constants are chosen in accordance with [11] and are given in Table 2.

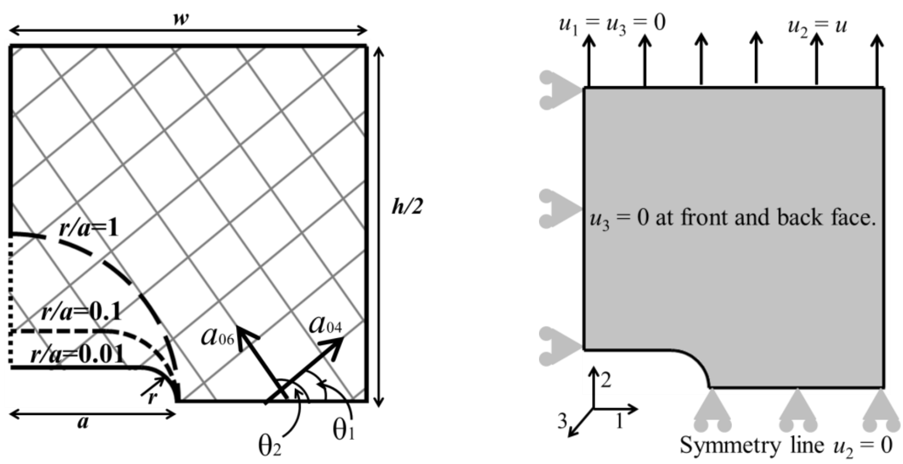

(a) (b)

Fig. 2: Schematic showing (a) notch geometry and fiber orientation ahead of notch defined by unit vectors a_{04}, a_{06} and (b) boundary conditions used in Abaqus finite element simulations.

Table 2. Material parameter used in FE simulations of skin type material [6, 11].

constants	μ_0 (MPa)	k_0 (MPa)	k_1 (MPa)	k_2	θ_1	θ_2
Isotropic	0.05	1	0	100	N/A	N/A
Anisotropic	0.05	1	1	100	45,60,0	135,120,90

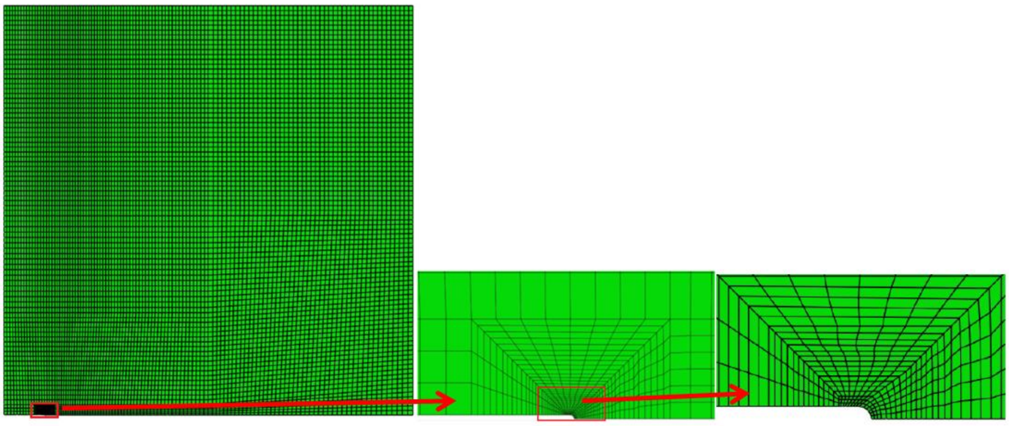

Fig. 3: Graded meshing used in FE simulations with finer mesh near the notch tip and a coarser mesh away from it.

The behavior of notch as a function of fiber orientation and notch geometry is compared through computation of the J-integral [25]. It is one of the most widely used fracture parameter to study the behavior of cracks and notches in isotropic materials [28-33]. Budiansky and Rice [34] extended the J-integral concept to anisotropic material and proposed J_k integral based on the conservation laws discussed in [35]. For a planar path, J_k is composed of two components J_1 and J_2. The first component J_1 is the well-known J-integral which provides the energy release rate associated with collinear crack extension, *i.e.* crack extension in the direction – 1 in Fig. 4. The second component J_2 yields the energy release rate associated with the crack extension orthogonal to the notch, *i.e.* in the direction – 2 in Fig. 4 [36, 37]. Hellen and Blackburn [36] concluded that a crack extends in the direction $\tan^{-1} J_2/J_1$ from axis-1 with energy release rate of $(J_1^2 + J_2^2)^{1/2}$ in mixed mode problems and cracks in anisotropic materials. The J_k integral approach has been used to study the fracture in anisotropic [38-40] and composite materials [41-43]. The same J_k approach is applied in the current study to investigate the behavior of a U-notch in hyperelastic anisotropic materials.

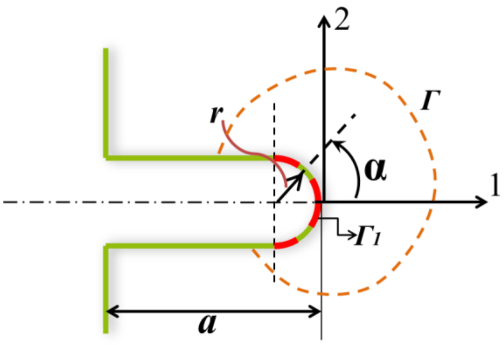

Fig. 4: Schematic showing notch geometry and contour path used to evaluate J-integral.

In summary, the J_k -integral at notch arc is evaluated according to [40, 44]. Briefly

$$J_k = \int_{\Gamma} \left(W n_k - \vec{T_i} \cdot \overrightarrow{\frac{\partial \boldsymbol{u_i}}{\partial \boldsymbol{x_k}}} \right) ds, (k = 1, 2) \tag{5}$$

where, n_k, u_i, T_i and W are the unit normal vector to the specified contour path Γ, displacement vector, traction vector and strain energy density, respectively. For a circular path at a distance r from the center of notch arc, we have $ds = r\, d\alpha, n_1 = \cos\alpha$ and $n_2 = \sin\alpha$. Now J_1 can be expanded as,

$$J_1 = \int_{\Gamma_1} \left(W n_1 - \vec{T} \cdot \overrightarrow{\frac{\partial \boldsymbol{u}}{\partial \boldsymbol{x}}} \right) ds = r \int_{-\pi}^{\pi} \left[W(\alpha)\cos\alpha - T(r,\alpha) \frac{du}{dx}(r,\alpha) \right] d\alpha \tag{6}$$

Taking notch arc as J path in Fig. 4 and realizing that $\vec{T} = 0$ on traction free notch surface, we get

$$J_1 = \int_{-\pi/2}^{\pi/2} W(\alpha) r \cos\alpha \, d\alpha. \tag{7}$$

Following similar steps, the expression for J_2 integral is,

$$J_2 = \int_{-\pi/2}^{\pi/2} W(\alpha) r \sin\alpha \, d\alpha. \tag{8}$$

Knowing the stress and strain fields from FEM simulations, the stain energy density is calculated using the relation

$$W = \int_0^{\varepsilon_{ij}} \boldsymbol{\sigma}_{ij} d\boldsymbol{\varepsilon}_{ij} \quad , \tag{9}$$

and the equivalent J- integral is obtained as

$$J = \sqrt{J_1^2 + J_2^2}. \tag{10}$$

4. Results and discussion

Before studying the notch behavior, it is necessary to perform a mesh convergence analysis by recording the variation in J-integral as a function of number of elements at the notch arc, as shown in Fig. 5. The region used to evaluate the J-integral is marked by a red line in Fig. 5(a). The other geometric parameter of the model are kept fixed at $r/a = 0.1$, $a/w = 0.1$ and $h/w = 2$. It should be noted that in this calculation only isotropic material properties are used in UMAT. Initially, the J value increases with increasing number of elements along the notch, but a converged solution is subsequently identified. The element size corresponding to a converged J-integral is found to be approximately 0.07 mm. Consequently, the element size at the notch edge is kept lower than 0.07 mm for the remainder of this study.

The accuracy of the numerical implementation followed in this study is further established by comparing the J-integral for a crack computed using UMAT to that calculated directly by the Abaqus, again for the simple case of isotropic neo-Hookean material model (parameters listed in Table 1). Fig. 6 demonstrates that the UMAT based J-integral calculation is accurate and can reliably be implemented for anisotropic hyperelasticity.

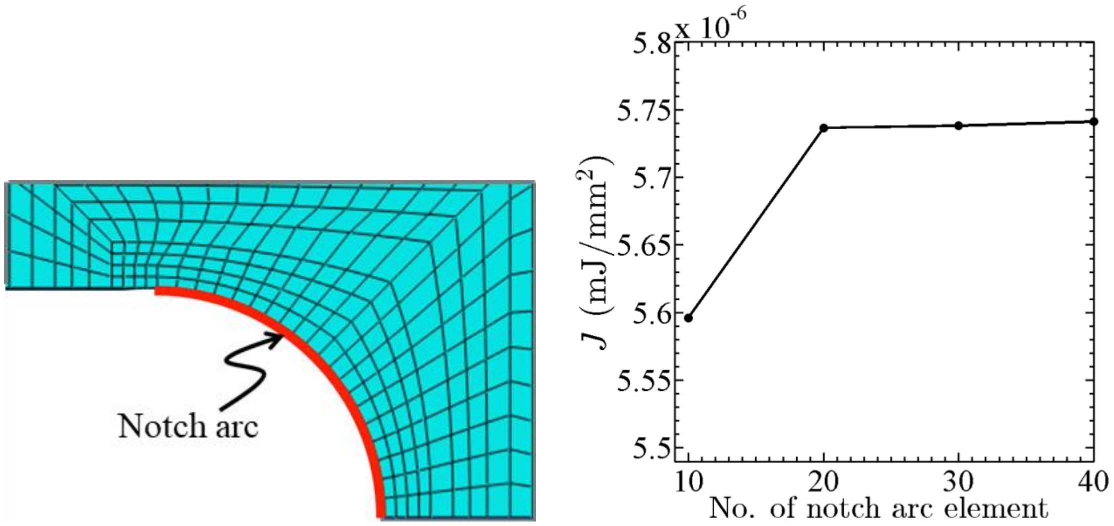

(a) (b)

Fig. 5: (a) Meshed model near the notch and (b) variation of J with number of elements at notch arc marked by red color curve in (a).

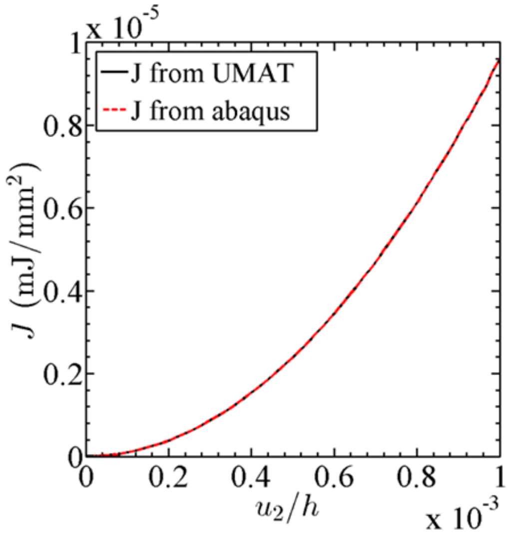

Fig. 6: Comparison of J energy obtained directly from Abaqus and calculated using output of FE simulations carried out using UMAT for a sharp crack in isotropic hyperelastic material with h/w=2 and a/w= 0.1.

Parametric investigation

A parametric study is next presented to examine the effect of fiber orientation and notch root radius on the behavior of U-notch in skin type materials. To this end, evolution of notch tip stress, anisotropic energy ϕ_{aniso} and the J-integral is compared for a range of cases. Even though these parameters are related, they are required for better understanding of effect of fiber induced anisotropy on the notch behavior in soft tissues. While σ_{22} provides the stress ahead of the notch tip and along the notch arc, J integral estimates the energy associated with the notch extension in soft tissue. Evolution of ϕ_{aniso} is important to characterize the relative contribution of anisotropic energy to the resistance of soft tissues against notch extension.

4.1. Effect of fiber orientation

The effect of anisotropic fiber orientation on the stiffening behavior of hyperelastic isotropic matrix is studied under tensile loading. Fig. 7 compares the variation of nominal stress ($\sigma_{\text{nom}} = \frac{F_R}{wt}$ with F_R being the total reaction force) as a function of nominal displacement u_2/h for three fiber families with orientations of 0-90°, 60-120° and 45-135° with respect to the 1–axis. As expected, higher fibre alignment with the direction of applied loading results in a stiffer material response.

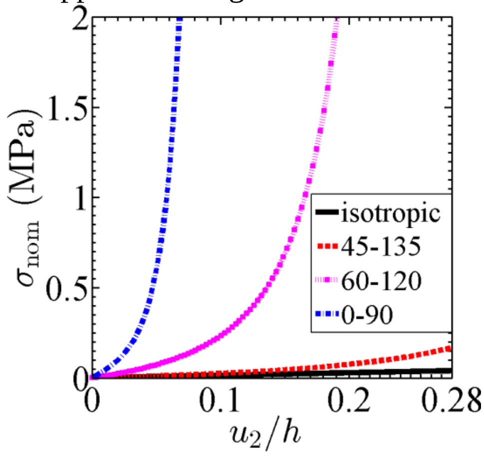

Fig. 7: Effect of fiber orientation on the evolution of nominal stress as a function of nominal displacement under tensile loading.

The effect of fiber orientation on the notch tip stress is studied next and the σ_{22} contours corresponding to this analysis are shown in Fig. 8 for a constant r/a = 0.1. For comparison, the variation of σ_{22} ahead of the notch in isotropic case is also included in Fig. 8. The local angular coordinate α is conveniently defined to refer locations along the notch arc, as illustrated in Fig. 8(a). In accordance with the established theory [45], σ_{22} is maximum just ahead of the notch tip at $\alpha = 0°$. The σ_{22} remains highest at $\alpha = 0°$ for the case of two orthogonal fibre families with initial orientations of 0 ° and 90 ° (i.e. 0-90° fibres). However, σ_{22} is maximum at $\alpha = 30°$, and 45° for fiber families oriented at 60-120°, 45-135° respectively. While the contour levels for isotropic case are shown in the inset of Fig. 8(a), a different set of contour levels are used for all anisotropic cases and are shown besides Fig 8(d).

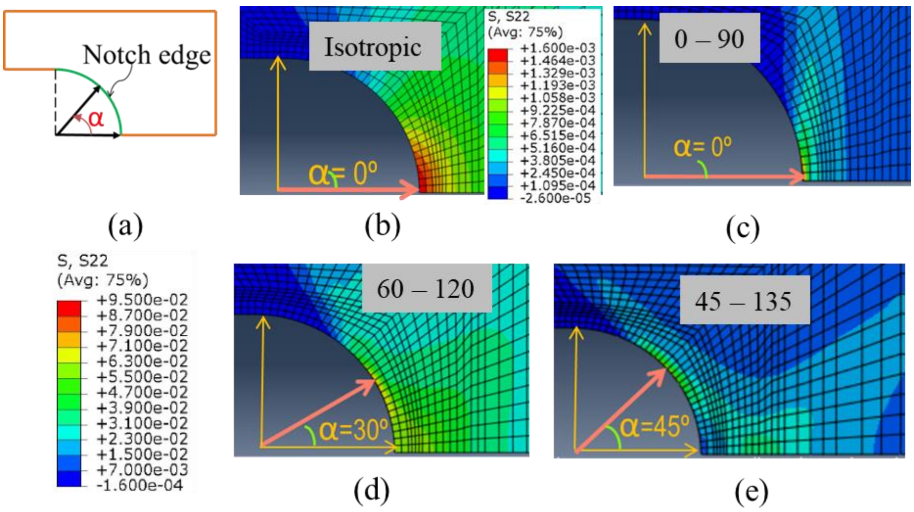

Fig. 8: (a) Schematic showing definition of angle α along the notch arc and σ_{22} contours near the notch tip for (b) isotropic and anisotropic material with fiber orientation of (c) 0-90 (d) 60-120 (e) 45-135. The geometric parameters are kept fixed at r/a =0.1, a/w = 0.1 and h/w = 2.

The corresponding variation of σ_{22} along the notch arc is presented in Fig. 9(a). The comparison of σ_{22} shown in Fig. 9(a) agrees with the observations recorded in σ_{22} contour plots in Fig. 8. The effect of notch root radius on the distribution of σ_{22} along notch arc is further investigate by repeating the FEM simulations for r/a = 0.01 and 1 in Fig. 9(b) and 9(c) respectively. Consistent with the theoretical predictions, while σ_{22} is higher for sharper notch (r/a = 0.01), it decreases for a relatively blunt notch having r/a = 1 for a fixed fiber orientation. It is to be noted here that even though the magnitude of σ_{22} changes with notch geometry in Fig. 9 (b-c), the qualitative variation of σ_{22} along the notch remains same as recorded in Fig. 9 (a).

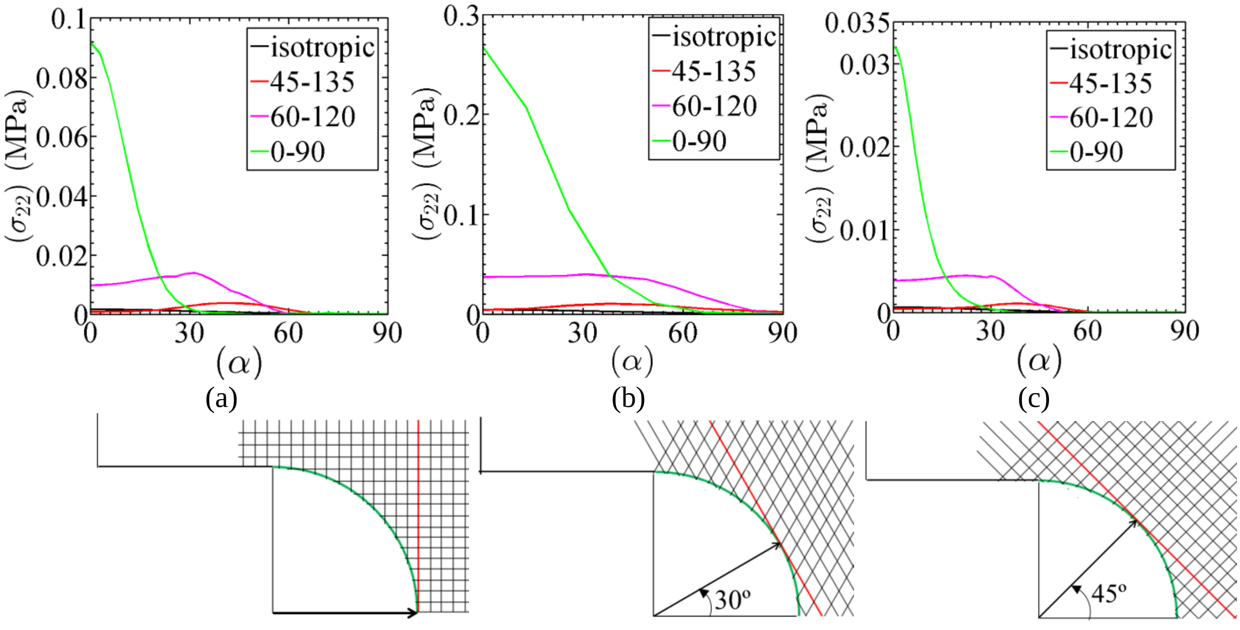

Fig. 9: Distribution of stress component σ_{22} along the notch edge for isotropic and anisotropic material with a/w = 0.1 and h/w = 2 and (a) r/a =0.1, (b) r/a =0.01, (c) r/a =1. Schematic of the notch edge with fiber orientation of (d) 0-90 (e) 60-120 (f) 45-135.

These observations are explained through schematics illustrations shown in Fig. 9 (d-f). The stiffer fibers oppose the deformation and provide resistance against notch extension under the applied loading. The fibers which are oriented perpendicular to the notch tip will be most effective in resisting the deformation. Therefore, σ_{22} will be maximum along the direction which is normal to the fiber orientation in Fig. 8. These fibers are shown by red color line and the angle made by the perpendicular to these fibers is in agreement with the observations recorded in Fig. 8 and 9 (a-c).

Next, the variation of σ_{22} along the notch bisector line is compared for different fiber orientations with varying r/a ratio in Fig. 10. While σ_{22} found to be maximum just at the notch tip for isotropic and 0-90 fiber orientation, it attains maximum value at some distance away from the notch tip for fiber orientations of 60-120° and 45-135°. This becomes more significant at higher r/a ratio of 0.1 and 1 in comparison to r/a = 0.01.

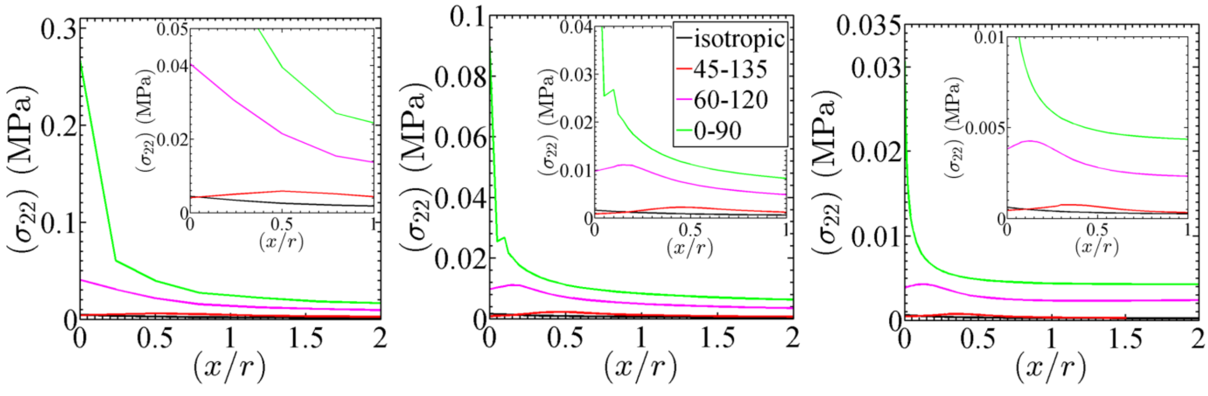

(a) (b) (c)

Fig. 10: Variation of stress component σ_{22} along the notch bisector line ahead of notch tip for isotropic and anisotropic material with (a) *r/a* =0.01, (b) *r/a* =0.1, (c) *r/a* =1.

This can be understood by finding the location of point where red color line intersects with the notch bisector line in Fig. 9(d-f). A simple trigonometric calculation provides the location of intersection point as $x = r(1\text{-}cos(\alpha))/cos(\alpha)$. Putting the angle α in this relation predicts that σ_{22} will be maximum at x/r = 0, 0.16 and 0.41 for fiber orientation of 0-90°, 60-120°, 45-135° respectively on the notch bisector line which is same as observed in Fig.10. Moreover, as *r/a* increases, the notch approaches the geometry of a circular hole leading to reduced stress concentration ahead of the notch tip and thus decreasing σ_{22} with increasing *r/a* ratios in Fig. 9 and 10.

The effect of fiber induced anisotropy on the stress along the notch arc is studied by comparing the variation of anisotropic energy in Fig. 11. In line with the observation for σ_{22}, the anisotropic energy ϕ_{aniso} along the notch arc is maximum at α = 0°, 30°, and 45° for fibers oriented at 0-90°, 60-120°, 45-135° respectively. This is due to the fact that the contribution of anisotropic energy from the fibers will be maximum at these angles along the notch arc as discussed earlier and shown in Fig. 9. Moreover, while ϕ_{aniso} is largest for 0-90° fiber orientations near to $\alpha=0$, it decreases with increasing *r/a* for any given fiber orientation as also recorded for σ_{22} in Fig.10. This is in accordance with the observations recorded in Fig. 7 that anisotropic fibers are more effective when they are oriented at 0-90° ahead of a sharper notch.

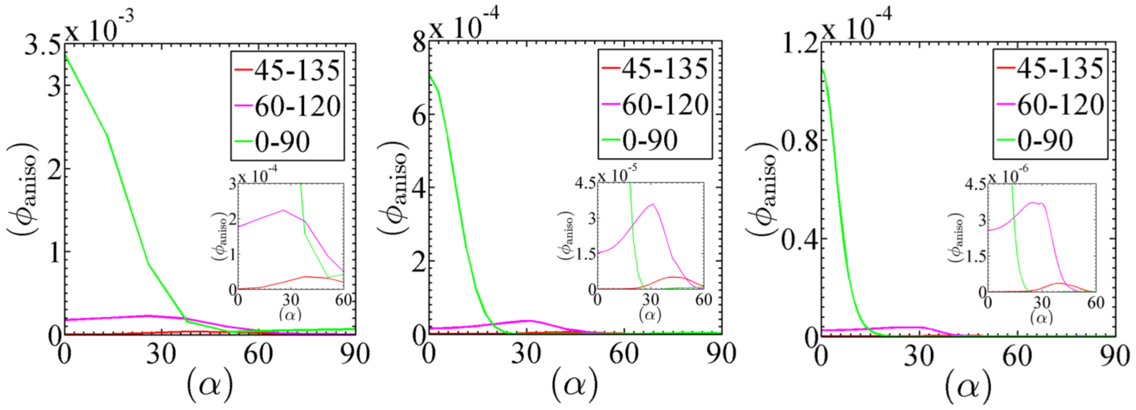

(a) (b) (c)

Fig. 11: Distribution of anisotropic energy along the notch arc for anisotropic material with (a) *r/a* =0.01, (b) *r/a* =0.1, (c) *r/a* =1.

The effect of fiber orientation on the notch behaviour in skin type material is further studied through the *J*-integral. The *J*-integral is calculated using the notch edge as the contour path for different fiber orientations and r/a ratios and its variation is compared in Fig. 12 as a function of applied displacement u_2. The J-integral increases significantly due to addition of fibers to an isotropic matrix. Moreover, the computed value of J is strongly dependent on the fibre orientation, with the highest value computed for the 0-90 fiber arrangement. It also implies that higher energy (or work done) may be needed for crack or notch propagation in hyperelastic materials reinforced with 0-90° fiber family in comparison to 45-135° and 60-120° fiber orientations. Consequently, the anisotropic fibers in a hyperelastic isotropic matrix tend to align perpendicular to notches (or cracks) to arrest their extension and contribute in high tearing strength of skin type materials. This provides a mechanistic explanation for the experimental observation of increased toughening due to fibre alignment ahead of a notch or crack-tip [20].

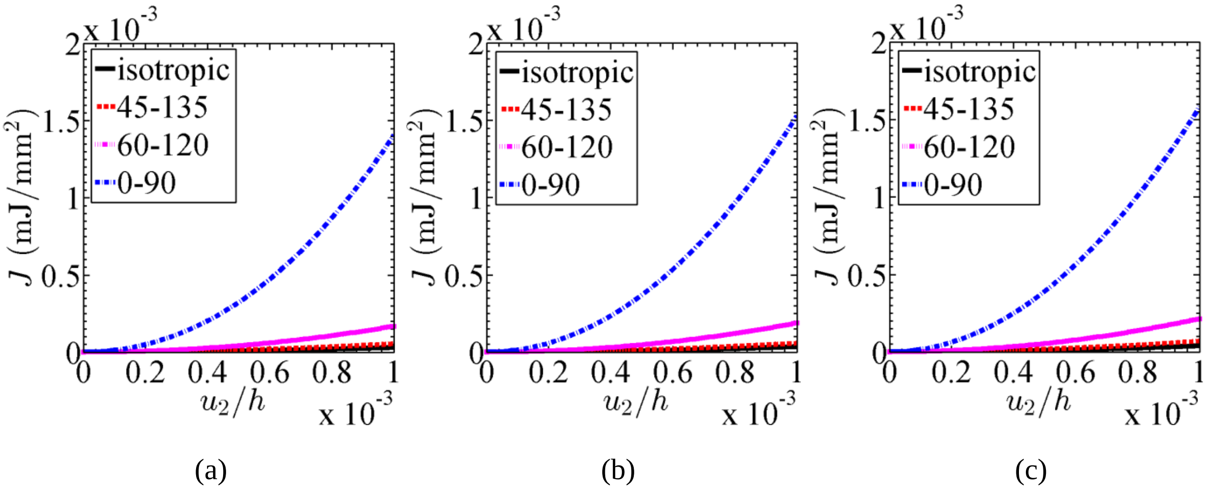

Fig. 12: Variation of J with u_2/h for different fiber orientation at (a) r/a =0.01, (b) r/a =0.1, (c) r/a =1.

Also of note, J increases nonlinearly with applied displacement u_2 for all fiber orientations. Initially, it is easier to deform the sample due to low fibre stress that is dominated by the matrix contribution. However, at larger values of applied displacements, fibers become increasingly aligned with the loading direction. Also, fibre extension results in significant strain stiffening. Such fibre alignment and strain stiffening significantly increase the resistance to deformation. This requires relatively higher energy to accommodate applied displacement and gives rise to the observed relationship between J and u_2.

The FEM simulations performed above reveals that introduction of anisotropic fibers significantly influence the stress field and J energy for U-notches in hyperelastic material. Moreover, localised regions of high anisotropic energy are computed close to the notch arc. Consequently, it is interesting to investigate the effect of anisotropic energy contribution on the J energy associated with the notch. Quantification of a meaningful measure of average anisotropic energy close to the notch tip is necessary to carry out such an analysis. Lazzarin and Berto [46] proposed a scheme for the averaging of strain energy in a finite volume through a material dependent parameter critical radius (R_C) which is independent of notch shape. R_C depends on the ultimate tensile strength and fracture toughness K_{IC} in some cases. Meybodi *et al.* [47] have extended the concept of R_C for the analysis of cracked rubbers. For hyperelastic materials, R_C is the maximum radius of a circle enclosing the region in which average of strain energy density is equal to the critical strain energy (Fig. 13(a)). Following this method, a region enclosed by circles of radius r and $\frac{r}{2}+R_C$ is chosen to compute the area average of anisotropic energy $\phi_{\text{aniso\_avg}} = \frac{\int \phi_{\text{aniso}}.d\Omega}{\Omega}$ near the notch arc in Fig. 13(b). R_C is taken in the direction of α_c (the angle of maximum σ_{22} from Fig. 9). To understand the relative contribution of anisotropic energy on the notch behaviour in skin type materials, a non- dimensional parameter ξ is defined by combining J, $\phi_{\text{aniso\_avg}}$ and R_C in eq. (10),

$$\xi = \frac{J}{(\phi_{\text{aniso-avg}})\times R_C} \tag{10}$$

It is to be noted here that the choice of ξ is just for analysis purpose and any other relevant definition of ξ may also serve this purpose.

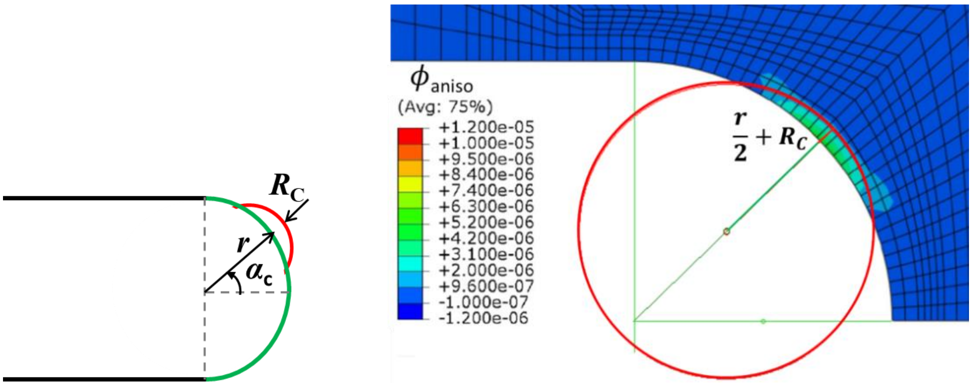

(a) (b)

Fig. 13: (a) Schematic showing location of critical radius R_C and (b) region around notch tip used to define $\phi_{aniso\text{-}avg}$ for fiber orientation of 45-135, a/w=0.1, h/w=2 and r/a =0.1.

Realizing that determining R_C is a prerequisite to calculate $\phi_{aniso\text{-}avg}$, the variation of ξ as a function of u_2/r is plotted in Fig. 14 for varying R_C/r values. Fig. 14(a) compares the variation of ξ for 45-135° fiber orientation. It shows that even though ξ decreases with increasing values of R_C/r, the qualitative behavior of ξ with u_2/h remains same. A similar behavior is recorded in Fig. 14(b) which compares the evolution of ξ for 0-90° fiber family. This analysis suggests that the exact value of R_C is not very critical for a qualitative analysis of ξ as a function of notch geometry parameters and fiber orientations. Therefore, the value of R_C/r = 0.05 is chosen as default in the remaining part of this section.

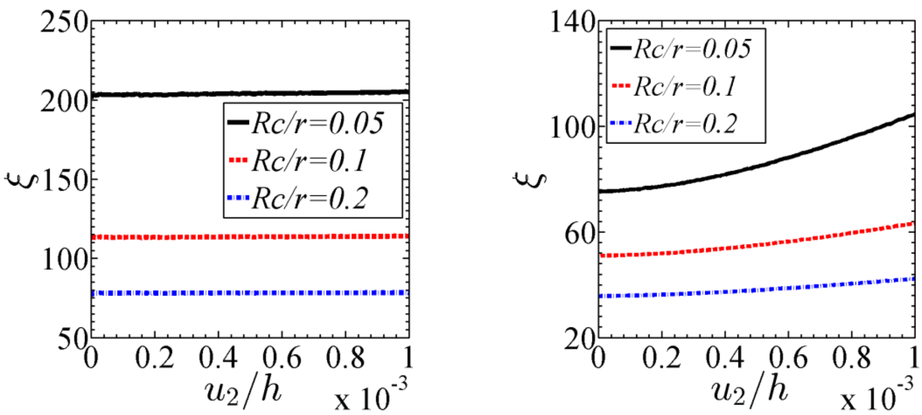

(a) (b)

Fig. 14: Variation of ξ with u_2/h at varying R_C/r ratio for fiber orientation of (a) 45-135, and (b) 0-90. The other parameters are kept constant at r/a =0.01, a/w=0.1, h/w=2.

Fig. 15 shows the effect of fiber orientation on the variation of ξ for different r/a ratio. In line with the observations made earlier, the contribution of anisotropic energy found to be highest for 0-90 and lowest for 45-135 fiber orientation at r/a = 0.01 in Fig. 15(a). Qualitatively similar trends with a relatively lower ξ for same u_2/h are observed at higher r/a = 0.1 and 1 in Fig. 15(b) and 15(c) respectively. This implies that the relative contribution of anisotropic energy due to fibers is higher for sharp notches in comparison to blunt notches. Moreover, as the notch root radius increases, both J and ϕ_{aniso} decrease, and therefore ξ also decreases at higher r/a at all fiber orientations considered in Fig. 15. Combining the observation of Fig. 15 with that of Fig. 7, 9 and 11, it is inferred that the higher anisotropic contribution for 0-90 fiber orientations provides increased resistance against notch extension in skin type materials.

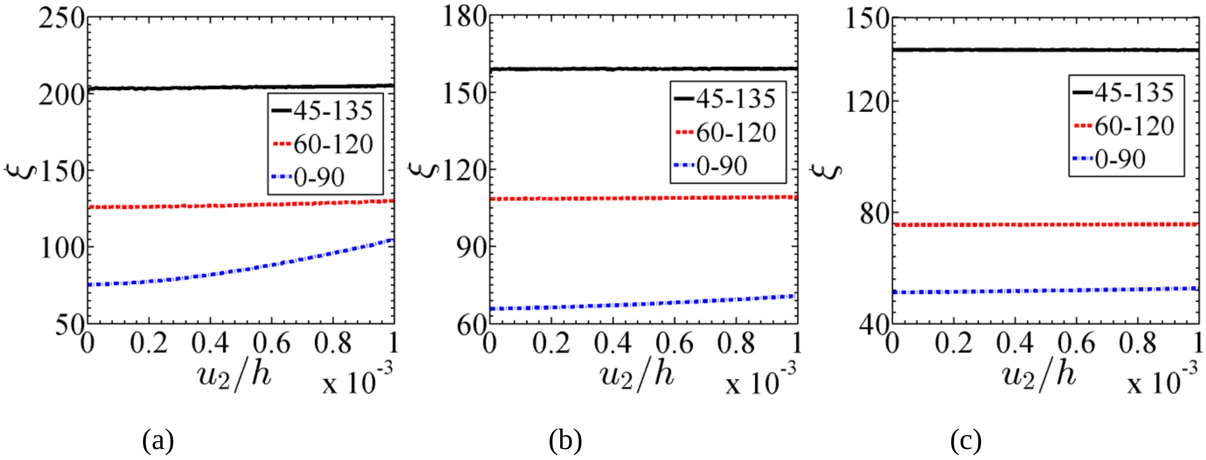

Fig. 15: Variation of ξ with u_2/h for (a) r/a =0.01, (b) r/a =0.1 and (c) r/a =1. The other parameters are a/w=0.1 and h/w=2 and R_C/r = 0.05.

Analysis of artery

Finally, we extend the investigations presented above to the analysis of arterial tissue. Experimental stress-strain data reported in [48] is used to determine the material parameters of MA model described in section 2. Nonlinear curve fitting is used in Fig. 16(a) to identify optimal anisotropic model using experimental test data in the circumferential and longitudinal directions [48]. The material properties, corresponding to medial layer, are found to be μ_0 = 0.007227 MPa, k_0 = 0.1783 MPa (corresponding to poison's ratio of 0.48), k_1 = 0.00754 MPa, k_2 = 380.64 with fiber orientation of 42°-138° provide a reasonable prediction of experimentally observed strain stiffening and anisotropy (see Fig 16(a)). To further understand the role of fiber anisotropy, the variation of J integral for two orthogonal notches (with fiber orientation 1 as 42 – 138 and orientation 2 as 132 – 228) in artery is compared in Fig. 16(b). Here again the orientation of fiber critically influence the J integral ahead of notch arc. Next, the influence of notch root radius on the variation of ξ for arterial tissue is predicted in Fig. 16(c). It follows the similar trends as observed in Fig. 15 for 45-135 fiber orientation. As r/a increases, ξ decreases and the contribution of anisotropic energy remains constant with u_2.

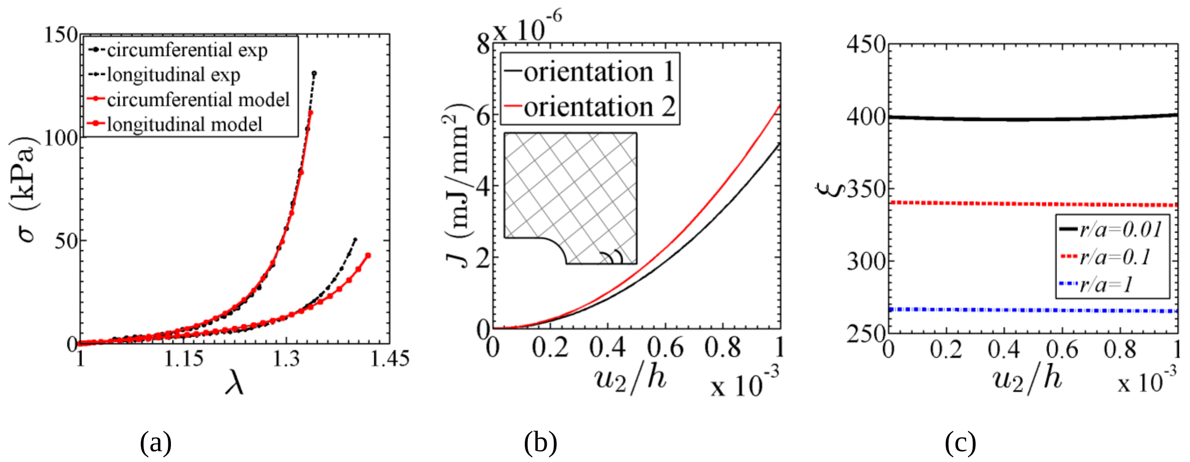

Fig. 16: (a) Comparison of stress-stretch plot obatined from FE simulation with experimental data reported in[48] for media layer of an artery. (b) variation of J with u_2/h for media layer for both orientation with notch geometry of r/a=0.1, (c) Variation of ξ with u_2/h for media layer with a/w=0.1, h/w=2 and R_C/r = 0.05.

5. Conclusion

Numerical analysis of U-notch in anisotropic hyperelastic materials is carried out using modified anisotropic (MA) model in FE simulations. An abaqus user defined material model UMAT is used to define the constitutive behavior of skin-type material. Simulation show that while stress σ_{22} is largest just ahead of the notch tip in isotropic materials, it attains maximum value at some distance away from notch tip in anisotropic materials. Moreover, σ_{22}, anisotropic energy ϕ_{aniso} and the J integral are found to be dependent on the orientation of anisotropic fibers ahead of the notch tip. It is observed that a 0-90 fiber orientation results in the highest stress at the notch, in addition to the highest anisotropic strain energy density, and the highest computed J-integral. To get a better insight on the contribution of anisotropic energy, a non-dimensional parameter $\xi = J/(R_C x(\phi_{\text{aniso}})_{avg})$ is defined to perform notch analysis in skin type materials. The evolution of ξ shows that while anisotropic energy contribution remains constant for 60-120° and 45-135° fiber orientations, it decreases for 0-90° fiber orientations with increasing applied displacement. In addition, the boundary effects also influence the stress field as well as ϕ_{aniso} ahead of the notch tip. As performing experiments on artery layers is very difficult, the developed model is used to predict the response of notch in medial layer of an artery under tensile loading. It is observed that the fiber orientation in medial layer is close to 45-135 fiber family and hence it follows similar trend that ξ remains constant with u_2 but decreases with an increase in notch root radius r. The insights gained from the numerical analysis performed in this study will not only lead to enhanced fracture resistance of artificial skin, it will also help in designing better skin healing strategies.

Acknowledgement: PKA acknowledge the financial support provided by IIT Ropar for summer visitation at Cambridge University, UK. PKA acknowledge and thank Prof. Vikram Deshpande, Department of Engineering, Cambridge University, UK for hosting me at his lab and having insightful discussions related to this work.

Reference

[1] S. C. B. Mannsfeld, B. C-K Tee, R. M. Stoltenberg, C. V. H-H Chen, S. Barman, B. V. O. Muir, A. N. Sokolov, C. Reese, Zhenan Bao, Highly sensitive flexible pressure sensors with microstructured rubber dielectric layers. Nature materials, 9(10), 859-864, (2010). https://doi.org/10.1038/nmat2834.

[2] T. I. Lee, W. S. Jang, E. Lee, Y. S. Kim, Z. L. Wang, H. K. Baik, J. M. Myoung, Ultrathin self-powered artificial skin. Energy & Environmental Science, 7(12) 3994-3999, (2014). https://doi.org/10.1039/C4EE02358G.

[3] S. Park, B. G. Shin, S. Jang, K. Chung, Three-dimensional self-healable touch sensing artificial skin device. ACS Applied Materials & Interfaces, 12(3), 3953-3960, (2020). https://doi.org/10.1021/acsami.9b19272.

[4] Alexander T. Trott, Wounds and Lacerations Emergency Care and Closure. Elsevier, 3rd Edition, (2005).

[5] I. V. Yannas , J. F. Burke , Design of an artificial skin. I. Basic design principles. Journal of Biomedical Materials Research, 14(1), 65-81, (1980). https://doi.org/10.1002/jbm.820140108.

[6] G. A. Holzapfel, T. C. Gasser, R. W. Ogden, A New Constitutive Framework for Arterial Wall Mechanics and a Comparative Study of Material Models. Journal of Elasticity, 61, 1–48, (2000). https://doi.org/10.1023/A:1010835316564.

[7] C. Valero, B. Navarro, D. Navajas, J. M. García-Aznar, Finite element simulation for the mechanical characterization of soft biological materials by atomic force microscopy. Journal of

the mechanical behavior of biomedical materials 62, 222-235, (2016). https://doi.org/10.1016/j.jmbbm.2016.05.006.
[8] P. W. Fok, K. Gou, Finite element simulation of intimal thickening in 2D multi-layered arterial cross sections by morphoelasticity. Computer Methods in Applied Mechanics and Engineering 363, 1-28 (2020). https://doi.org/10.1016/j.cma.2020.112860.
[9] E. Pena, A.P. Del Palomar, B. Calvo, M. Martı´nez, M. Doblare, Computational modeling of diarthrodial Joints. Physiological, pathological and post-surgery simulations. Archives of Computational Methods in Engineering, 14, 47–91 (2007). https://doi.org/10.1007/s11831-006-9001-3.
[10] L. Vergori, M. Destrade, P. McGarry, R. W. Ogden, On anisotropic elasticity and questions concerning its Finite Element implementation. Computational Mechanics 52, 1185-1197, (2013). https://doi.org/10.1007/s00466-013-0871-6.
[11] D. R. Nolan, A. L. Gower, M. Destrade, R.W.Ogden, J. P. McGarry, A robust anisotropic hyperelastic formulation for the modeling of soft tissue. Journal of the mechanical behavior of biomedical materials, 39, 48-60, (2014). https://doi.org/10.1016/j.jmbbm.2014.06.016.
[12] J. M. Benítez, F. J. Montáns, The mechanical behavior of skin: Structures and models for the finite element analysis. Computers & Structures, 190, 75-107, (2017). https://doi.org/10.1016/j.compstruc.2017.05.003.
[13] L-C. Gerhardt, J. Schmidt, J. A. Sanz-Herrera, F. P. T. Baaijens, T. Ansari, G. W. M. Peters, C. W. J. Oomens. A novel method for visualising and quantifying through-plane skin layer deformations. Journal of the mechanical behavior of biomedical materials, 14, 199-207 (2012). https://doi.org/10.1016/j.jmbbm.2012.05.014.
[14] T. Lee, A. K. Gosain , I. Bilionis, A. B. Tepole, Predicting the effect of aging and defect size on the stress profiles of skin from advancement, rotation and transposition flap surgeries. Journal of the Mechanics and Physics of Solids, 125, 572-590 (2019). https://doi.org/10.1016/j.jmps.2019.01.012.
[15] Z. Zhu, C. Jiang, H. Jiang, A visco-hyperelastic model of brain tissue incorporating both tension/compression asymmetry and volume compressibility. Acta Mechanica 230(6), 2125-2135 (2019). https://doi.org/10.1007/s00707-019-02383-1.
[16] D. R. Nolan, C. Lally, An investigation of damage mechanisms in mechanobiological models of in-stent restenosis. Journal of computational science 24, 132-142 (2018). https://doi.org/10.1016/j.jocs.2017.04.009.
[17] P. S. Zun, , T. Anikina, , A. Svitenkov, and A. G. Hoekstra, A comparison of fully-coupled 3D in-stent restenosis simulations to in-vivo data. Frontiers in physiology 8, (2017). https://doi.org/10.3389/fphys.2017.00284.
[18] F. Levrero-Florencio, F. Margara, E. Zacur, A. Bueno-Orovio, Z. J. Wang, A. Santiago, J. Aguado-Sierra, G. Houzeaux , V. Grau , D. Kay , M. Vázquez, R. Ruiz-Baier , B. Rodriguez, Sensitivity analysis of a strongly-coupled human-based electromechanical cardiac model: Effect of mechanical parameters on physiologically relevant biomarkers. Computer Methods in Applied Mechanics and Engineering 361 (2020). https://doi.org/10.1016/j.cma.2019.112762.
[19] A. Ahmadi, and M. Asgari, Nonlinear coupled electro-mechanical behavior of a novel anisotropic fiber-reinforced dielectric elastomer. International Journal of Non-Linear Mechanics 119, (2020). https://doi.org/10.1016/j.ijnonlinmec.2019.103364.
[20] W. Yang, V. R. Sherman, B. Gludovatz, E. Schaible, P. Stewart, R. O. Ritchie and M. A. Meyers, On the tear resistance of skin. Nature communications 6, 6649, (2015). https://doi.org/10.1038/ncomms7649.
[21] M. Ovaska , Z. Bertalan , A. Miksic *et. al.*, Deformation and fracture of echinoderm collagen networks. Journal of the Mechanical Behavior of Biomedical Materials 65, 42-52, (2017). https://doi.org/10.1016/j.jmbbm.2016.07.035.

[22] K. Bircher, M. Zündel, M. Pensalfini, et al. Tear resistance of soft collagenous tissues. Nature communications 10, 792 (2019). https://doi.org/10.1038/s41467-019-08723-y.
[23] Q. Meng , B. Li , T. Li , X. Q. Feng, Effects of nanofiber orientations on the fracture toughness of cellulose nanopaper. Engineering Fracture Mechanics 194, 350-361, (2018). https://doi.org/10.1016/j.engfracmech.2018.03.034.
[24] D. J. Lee, J. A. Donovan, Critical *J*-integral and tearing energies for fracture of reinforced natural rubber. Theoretical and applied fracture mechanics 4, 137-147, (1985). https://doi.org/10.1016/0167-8442(85)90018-7.
[25] J. R. Rice, A Path Independent Integral and the Approximate Analysis of Strain Concentration by Notches and Cracks. Journal of Applied Mechanics, 379-386, (1968). https://doi.org/10.1115/1.3601206.
[26] D. R. Nolan, J. P. McGarry, On the compressibility of arterial tissue. Annals of biomedical engineering 44 (4), 993-1007, (2016). https://doi.org/10.1007/s10439-015-1417-1.
[27] Simulia, 2016. Abaqus/CAE User's Manual, Version 6.14.
[28] G. Cherepanov, The propagation of cracks in a continuous medium. Journal of Applied Mathematics and Mechanics 31, 503-512, (1967). https://doi.org/10.1016/0021-8928(67)90034-2.
[29] Y. H. Chen, T. J. Lu, On the path dependence of the J-integral in notch problems. International Journal of Solids and Structures, 41, 607–618, (2004). https://doi.org/10.1016/j.ijsolstr.2003.10.007.
[30] Y. G. Matvienko, E. Morozov, Calculation of the energy J-integral for bodies with notches and cracks. International Journal of Fracture 125, 249-261, (2004). https://doi.org/10.1023/B:FRAC.0000022241.23377.91.
[31] F. Berto, P. Lazzarin, Y. G. Matvienko, J-integral evaluation for U- and V-blunt notches under Mode I loading and materials obeying a power hardening law. International Journal Fracture 146, 33–51, (2007). https://doi.org/10.1007/s10704-007-9134-x.
[32] P. Livieri, Use of J-integral to predict static failures in sharp V-notches and rounded U-notches. Engineering Fracture Mechanics 75, 1779–1793, (2008). https://doi.org/10.1016/j.engfracmech.2007.01.022.
[33] E. Barati, Y. Alizadeh, J. A. Mohandesi, Relationship between J-integral and averaged strain-energy density for U-notches in the case of large control volume under Mode I loading. Engineering Fracture Mechanics 78, 1317–1322, (2011). https://doi.org/10.1016/j.engfracmech.2011.01.017.
[34] B. Budiansky and J. R. Rice, Conservation laws and energy release rates. Journal of Applied Mechanics 40, 201-203, (1973). https://doi.org/10.1115/1.3422926.
[35] J. K. Knowles and E. Sternberg, On a class of conservation laws in linearized and finite elastostatics. Archive for Rational Mechanics and Analysis 44, 187-211, (1972). https://doi.org/10.1007/BF00250778.
[36] T. K. Hellen and W. S. Blackburn, The calculation of stress intensity factors for combined tensile and shear loading. International Journal of Fracture 11, 605-617, (1975). https://doi.org/10.1007/BF00116368.
[37] K. Y. Lee, Contradiction of J_k integral. International Journal of Fracture 31, 53-54, (1986). https://doi.org/10.1007/BF00018932.
[38] P. O. Judt, J. C. Zarges, A. Ricoeur, H. P. Heim, Anisotropic fracture properties and crack path prediction in glass and cellulose fiber reinforced composites. Engineering Fracture Mechanics 188, 344–360, (2018). https://doi.org/10.1016/j.engfracmech.2017.08.027.
[39] P. O. Judt, J. C. Zarges, A. Ricoeur, H. P. Heim, Crack path predictions in fiber reinforced composites. Procedia Structural Integrity 5, 769-776, (2017). https://doi.org/10.1016/j.prostr.2017.07.168.

[40] P. Sollero, M.H. Aliabadi, Fracture mechanics analysis of anisotropic plates by the boundary element method. International Journal of Fracture 64, 269-284, (1993). https://doi.org/10.1007/BF00017845.

[41] A. Tafreshi, Computation of the Jk-integrals for bimaterial interface cracks using boundary element crack shape sensitivities. Theoretical and Applied Fracture Mechanics 82, 77-87, (2016). https://doi.org/10.1016/j.tafmec.2015.12.003.

[42] S. J. Chu, C. S. Hong, Application of the J_k integral to mixed mode crack problems for anisotropic composite laminates. Engineering Fracture Mechanics 35(6), 1093-1103 (1990). https://doi.org/10.1016/0013-7944(90)90137-6.

[43] M. H. Aliabadi, M. Guagliano, Fracture and Damage of Composites. WIT Transactions on State-of-the-art in Science and Engineering, 8th Edition, (2006).

[44] H. R. Majidi, A.R. Torabi, M.E. Golmakani, J-integral expression for mixed mode I/II ductile failure prediction of U-notched Al 6061-T6 plates under large-scale yielding regime. Engineering Fracture Mechanics 195, 253–266, (2018). https://doi.org/10.1016/j.engfracmech.2018.04.007.

[45] A. Khechai, A. Tati, B. Guerira, A. Guettala, P.M. Mohite, Strength degradation and stress analysis of composite plates with circular, square and rectangular notches using digital image correlation. Composite Structures, 185, 699–715 (2018). https://doi.org/10.1016/j.compstruct.2017.11.060.

[46] P. Lazzarin, , F. Berto, Some Expressions for the Strain Energy in a Finite Volume Surrounding the Root of Blunt V-notches. International Journal of Fracture 135, 161–185, (2005). https://doi.org/10.1007/s10704-005-3943-6.

[47] M. Heydari-Meybodi, M.R. Ayatollahi, F. Berto, Averaged strain energy density criterion for rupture assessment of cracked rubbers: A novel method for determination of critical SED. Engineering Fracture Mechanics 190, 93–103, (2018). https://doi.org/10.1016/j.engfracmech.2017.12.006.

[48] G A. Holzapfel, G. Sommer, C. T. Gasser, P. Regitnig, Determination of layer-specific mechanical properties of human coronary arteries with nonatherosclerotic intimal thickening and related constitutive modeling. American Journal of Physiology-Heart and Circulatory Physiology 289, H2048–H2058, (2005). https://doi.org/10.1152/ajpheart.00934.2004.